mum rate occurring at closest approach (*7*). The radio waves group reported an upper limit to the dust flux for particles with mass exceeding 10^{-10} g that is 100 times lower than the predicted flux (*3*).

Shortly after the ICE encounter, comets Giacobini-Zinner and Halley were near each other in the sky. Figure 4 shows the symbolic changing of the guard.

The ICE spacecraft will be about 0.2 AU upstream from comet Halley in late March 1986. Disturbances and changes in the solar wind observed by ICE should be related to the behavior of Halley's ion tail observed from Earth by members of the International Halley Watch. Given the large distance from which comet Giacobini-Zinner was first detected by ICE and the expected factor of 10 larger gas production rate for comet Halley, it is possible that ICE will detect comet Halley itself.

REFERENCES AND NOTES

1. *Geophys. Res. Lett.* **11**, 1027 (1984).
2. R. Farquhar, D. Muhonen, L. C. Church, *J. Astronaut. Sci.* **33**, No. 3 (1985).
3. D. K. Yeomans and J. C. Brandt, *The Comet Giacobini-Zinner Handbook* (NASA/Jet Propulsion Laboratory, Pasadena, CA, 1985).
4. T. T. von Rosenvinge and J. C. Brandt, *Eos* **66**, 625 (1985).
5. *IEEE Trans. Geosci. Electron.* **GE-16** (1978).
6. A. I. F. Stewart, M. R. Combi, W. H. Smyth, *Bull. Am. Astron. Soc.* **17**, 686 (1985).
7. F. L. Scarf *et al.*, *Science* **232**, 377 (1986).
8. R. J. Hynds, S. W. H. Cowley, T. R. Sanderson, K.-P. Wenzel, J. J. Rooijen, *ibid.*, p. 361.
9. F. M. Ipavich *et al.*, *ibid.*, p. 366.
10. S. J. Bame *et al.*, *ibid.*, p. 356.
11. E. J. Smith *et al.*, *ibid.*, p. 382.
12. N. Meyer-Vernet *et al.*, *ibid.*, p. 370.
13. H. Alfvén, *Tellus* **9**, 92 (1957).
14. K. W. Ogilvie *et al.*, *Science* **232**, 374 (1986).
15. F. L. Whipple, *Astrophys. J.* **111**, 375 (1950).
16. N. T. Bobrovnikoff, *ibid.* **66**, 439 (1927).

17. The success of this mission depended on the cooperation of many individuals in the face of the unknown and with a fixed deadline. At the risk of omission, we thank R. Amorose, P. Astill, J. Corrigan, J. Day, Jr., D. Dunham, J. Elliott, N. Fanelli, L. Hatakeyama, J. King, J. Madden, S. Maran, W. Martin, D. Muhonen, E. Nace, M. Niedner, R. Schumacher, J. Spohr, M. Titland, R. Wales, M. Ward, J. Wolfe, and D. Yeomans.

7 January 1986; accepted 31 January 1986

Comet Giacobini-Zinner: Plasma Description

S. J. Bame, R. C. Anderson, J. R. Asbridge, D. N. Baker, W. C. Feldman, S. A. Fuselier, J. T. Gosling, D. J. McComas, M. F. Thomsen, D. T. Young, R. D. Zwickl

A strong interaction between the solar wind and comet Giacobini-Zinner was observed on 11 September 1985 with the Los Alamos plasma electron experiment on the International Cometary Explorer (ICE) spacecraft. As ICE approached an intercept point 7800 kilometers behind the nucleus from the south and receded to the north, upstream phenomena due to the comet were observed. Periods of enhanced electron heat flux from the comet as well as almost continuous electron density fluctuations were measured. These effects are related to the strong electron heating observed in the cometary interaction region and to cometary ion pickup by the solar wind, respectively. No evidence for a conventional bow shock was found as ICE entered and exited the regions of strongest interaction of the solar wind with the cometary environment. The outer extent of this strong interaction zone was a transition region in which the solar wind plasma was heated, compressed, and slowed. Inside the inner boundary of the transition region was a sheath that enclosed a cold intermediate coma. In the transition region and sheath, small-scale enhancements in density were observed. These density spikes may be due to an instability associated with cometary ion pickup or to the passage of ICE through cometary ray structures. In the center of the cold intermediate coma a narrow, high-density core of plasma, presumably the developing plasma tail, was found. In some ways this tail can be compared to the plasma sheet in Earth's magnetotail and to the current sheet in the tail at Venus. This type of configuration is expected in the double-lobe magnetic topology detected at the comet, possibly caused by the theoretically expected draping of the interplanetary magnetic field around its ionosphere.

The results of the Los Alamos plasma electron experiment obtained during the encounter of comet Giacobini-Zinner with the International Cometary Explorer (ICE) on 11 September 1985 indicate that the solar wind interacted strongly with the comet. During the encounter, the spacecraft passed through several distinctive plasma regimes. Some preliminary interpretations of the plasma electron data are presented here. It is expected that these interpretations will be refined as more in-depth analyses become available. In particular, future analyses that make use of the combined data of various experiments on ICE should lead to more detailed interpretations of the phenomena observed.

Instrumental details. Electron measurements were made with an electrostatic analyzer (*1*) composed of a spherical section analyzer with a 135° bending angle, followed by a system of secondary electron emitters and an electron multiplier that gives two- and three-dimensional capability. Only two-dimensional measurements of plasma electrons were made during the encounter so as to maximize the measurement repetition rate. A measurement cycle consists of 16 energy sweeps spaced uniformly throughout a 3-second spacecraft revolution. During each sweep, measurements are made at each of 15 energy levels. The experiment has two energy ranges: a "normal" range of 10 to 1000 eV and an infrequently used "photoelectron" range of 1.9 to 190 eV. The latter range was included for studying spacecraft charging, since a knowledge of the spacecraft potential is essential for analyzing low-energy electron data. At the encounter telemetry rate, one measurement cycle was obtained every 24 seconds, so the data format consists of 3-second data sets followed by 21-second gaps. In this report the data are presented in histograms in which the actual 3-second data acquisition times occur during the first 3 seconds of the 24-second-wide bars representing derived data points. In a few cases, abrupt changes in electron distributions occurred in times comparable to or less than the time between energy sweeps (~0.1 second). The plasma electron bulk flow speed, temperature, and density are determined by numerical integration of the entire plasma distribution.

The comet's plasma structure. Figure 1 shows a 10-hour plot of the electron moments during the solar wind–comet interaction (Fig. 1). The data extend from 0600 universal time (U.T.), when ICE was in the solar wind, through the central passage at ~1102 U.T., to 1600 U.T., when ICE was again in the solar wind. Shown are electron density (n), temperature (T), and plasma bulk speed (V), computed from the electron distributions. (The subscript e is to be understood for all the plasma moments throughout the text.) The data in Fig. 1 were processed through a three-point run-

University of California, Los Alamos National Laboratory, Los Alamos, NM 87545.

ning-average filter to improve the clarity of the presentation on this compressed scale. In the upstream region of the comet, periods of enhanced fluxes of energetic (>100 eV) electrons were observed streaming along the interplanetary magnetic field (IMF) in the direction opposite the heat flux from the solar corona (*2*). These counterstreaming electrons came from a hot source, associated with the comet, when the IMF connected the spacecraft with the solar wind–comet region in which the electrons were strongly heated. During these times of connection, moderate enhancements in the average value of T were observed.

Similar counterstreaming heat fluxes are observed upstream from Earth's bow shock when the IMF connects to the hot magnetosheath plasma behind the shock (*3*). Connection was demonstrated most convincingly by the existence of a counterstreaming electron distribution, since such distributions are only rarely observed away from planetary bodies. With the IMF direction alone, connection can only be inferred on the basis of an assumed configuration of the hot source. Also in the regions upstream from the comet, large fluctuations in electron density were present almost continuously.

Nearer to the comet, at ~0920 U.T., the average values of electron density and temperature, n_{av} and T_{av}, began to increase as ICE entered a region of strong interaction between the solar wind and cometary plasma. Before this region was entered, at ~0840 U.T., the bulk flow speed began to decrease, probably because of the increased pickup of cometary ions. ICE left the comet through a similar region at ~1220 U.T. Again, V_{av} did not reach its full undisturbed upstream solar wind value until ~1250 U.T., well after exiting the region. This behavior is reminiscent of solar wind slowing upstream from Earth's bow shock, associated with upstream ion events (*4*), although, as mentioned, the role of cometary ion pickup may be the dominant factor in the slowing at Giacobini-Zinner. The region in which n_{av} and T_{av} increase toward the center of the comet, while V_{av} decreases, is a transition region. There appears to be no evidence of a conventional bow shock at the edge or within the region. However, after traversing the transition region, the solar wind had been heated, compressed, and slowed. Closer to the time of closest approach (forward from ~1007 U.T. and backward from ~1148 U.T.), another plasma region was found in which V_{av} continued to decrease, while n_{av} and T_{av} began to decrease from their elevated transition region values. This region, in which the cometary plasma becomes increasingly important, has been termed a sheath because it surrounds a cold intermediate coma closer to the comet. Large fluctuations were superimposed on the slowly changing average values of density, temperature, and speed in both the transition region and the sheath (Fig. 1). These fluctuations may be the result of instabilities associated with cometary ion pickup (*5*), or they may be caused by ICE traversals of cometary rays or streamers.

Further inspection of Fig. 1 shows a distinctive region centered on the time of closest approach at ~1102 U.T. in which the electron temperature falls to below 50,000 K, density rises, and flow speed decreases to less than 30 km sec^{-1} (the accuracy of the measurement). We identify this denser, nearly stationary region as the intermediate coma to distinguish it from the larger coma identified in photographs and the inner coma in which important chemical processes are taking place. The data suggest that a boundary layer separates the sheath and the intermediate coma. Inbound, the boundary layer was found between ~1050 and ~1056 U.T., while outbound the limits

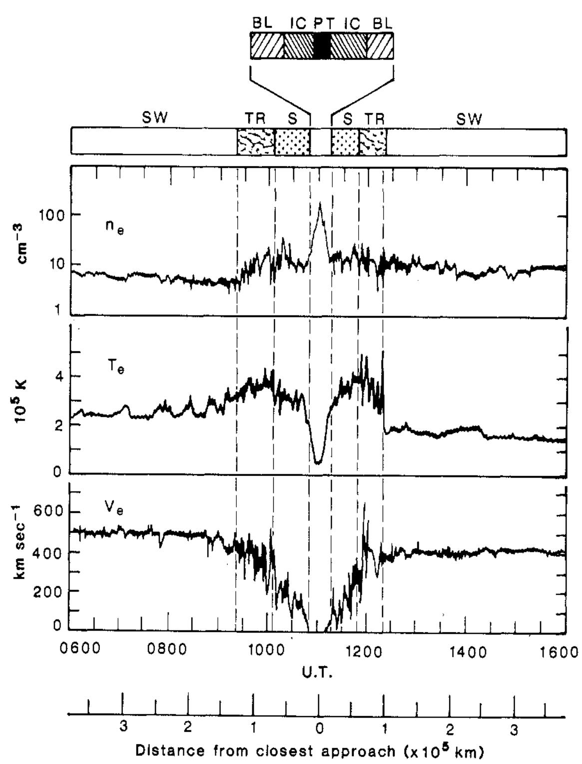

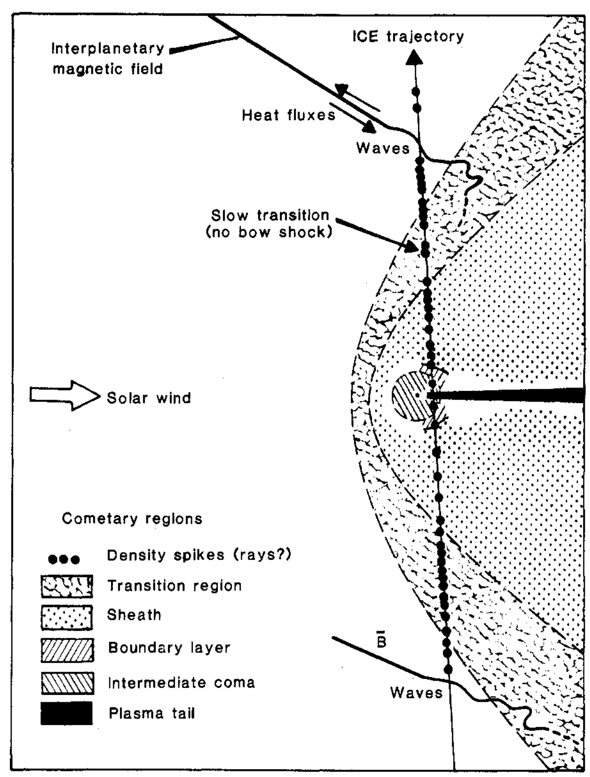

Fig. 1 (left). Overview plot of three-point running averages of electron density, temperature, and speed, measured during the encounter of ICE with comet Giacobini-Zinner. Plasma regions are identified at the top by SW, solar wind; TR, transition region; S, sheath; BL, boundary layer; IC, cold intermediate coma; and PT, plasma tail. Fig. 2 (right). Possible configuration of comet Giacobini-Zinner, based on the boundary data in Tables 1 and 2. Region coding is shown. The dots along the encounter path, which show the positions of density peaks, do not include some of the smaller peaks, particularly those in upstream regions. The size of the comet nucleus is exaggerated. ICE traversed the comet regions along a path almost perpendicular to the ecliptic, from south to north. Since boundary crossings were detected only along the trajectory, the shapes shown are mostly conjecture.

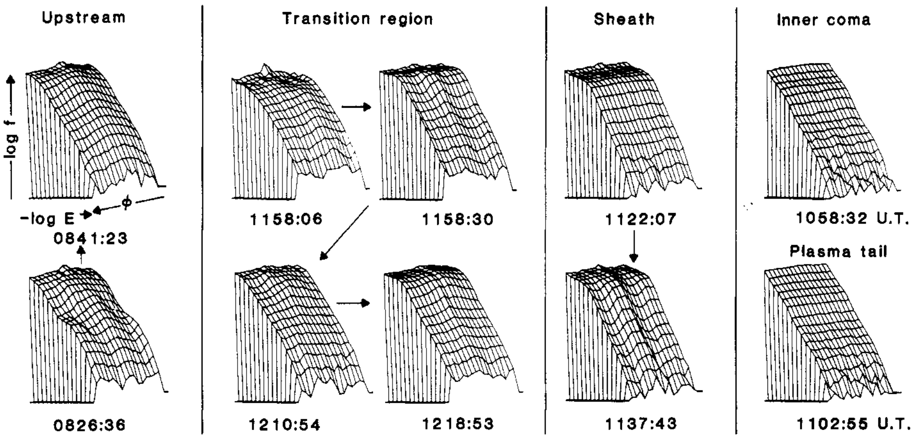

Fig. 3. Sample plasma electron velocity distributions measured in the solar wind and four of the cometary plasma regions during the passage of ICE. As shown, log $f(V)$ is plotted vertically; log E, along the visible horizontal axis; and the sweep angle, ϕ, transverse to log E. In each distribution the 16 energy spectra measured in one spacecraft revolution are represented by the descending traces, which together establish a curved surface as shown. A small sunward background shows as a bump at the lowest energies near the center of the distributions. The antisunward flow direction is located at the center of each distribution.

were ~1110 and ~1115 U.T. Centered on the time of closest approach was a well-defined, narrow, central region with very high density, which ICE passed through in 3 minutes. This cold, dense region may have been the developing plasma tail. The flow speed in the tail, within the accuracy of our experiment, was no greater than 30 km sec^{-1}. It is expected on the basis of optical observations that farther downstream in the fully developed tail the plasma flow speed must reach hundreds of kilometers per second. The plasma in the tail is presumed to be that necessary to sustain the double-lobe, magnetic neutral sheet configuration of the comet tail (*6*) that was detected at Giacobini-Zinner (*7*). Some theories predict such a configuration, caused by draping of the IMF around the ionosphere (*8*). The developing plasma tail serves a function at the comet similar to that of the current sheet in the magnetic tail of Venus (*9*) and the plasma sheet with embedded current sheet in Earth's magnetotail (*10*).

The boundary crossing times cited above were established not only with the overview data in Fig. 1, but also by detailed inspection of individual electron velocity distributions, which have distinctive features in the various regions. Boundary crossing times are given in Table 1, along with time intervals and the corresponding distances from closest approach. Table 2 gives distances across the outer boundaries of the regions and their average thicknesses along the ICE trajectory. Note that the 3000-km thickness of the plasma tail cited in Table 2 is an upper limit if the tail configuration is sheetlike and a lower limit if it has a near-circular cross section, since the crossing position and angle are unknown. A plasma configuration of the comet (Fig. 2) may be inferred on the basis of the dimensions given in the tables. The exact shapes of the regions are speculative, of course, since boundaries were established only along the path of ICE. The intermediate coma is depicted with a spherical configuration, while in fact it is probably distorted by solar wind and radiation pressure as well as by nonsymmetrical volatilization of frozen gases and dust (*11*). Comparisons with model calculations should help establish more realistic shapes.

Cometary heat fluxes in upstream regions. Events identified as IMF connections with the hot comet transition region are evident in the solar wind data for before and after the encounter. An inferred geometry of the IMF threading the spacecraft and connecting it to the transition region is shown in Fig. 2 for both the inbound and outbound regions. When connection occurred, energetic electrons reached the spacecraft along the IMF lines that penetrated the hot transition region.

Normally, when on unconnected lines, the electron angular distribution in the higher energy channels exhibited a single-peaked shape at constant energy. The distribution at 0841:23 U.T. shown in Fig. 3 exhibits such a single peak, which is due to an outflow of hot electrons from the solar corona. A moment plot (Fig. 4) shows that the heat flux direction projected into the ecliptic plane was 315° at that time. Its polar direction was not determined by the experiment in the two-dimensional operating mode. The distribution measured earlier at 0826:36 U.T. (Fig. 3) has a distinctly different character, displaying two peaks with ~180° separations in the angular distributions at higher energies. This distribution shows that heat fluxes from two different sources were counterstreaming along the IMF. As mentioned before, distributions of this type are common upstream from Earth's bow shock.

One source of heat flux is the solar corona, of course, while the other must be the hot cometary transition region. The connected distribution at 0826:36 U.T. was measured at a time when the direction of the net heat flux was ~180° away from the heat flux of the unconnected distribution at 0841:23 U.T. (Fig. 4). The 180° change indicates that the cometary heat flux is the dominant one. Another connection event between ~0848 and ~0855 U.T. is evident in Fig. 4. Superimposed and heat flux–aligned (equivalent to field-aligned) cuts through velocity distributions measured both before and after a brief connection event just before 0848 U.T. are shown in Fig. 5. This event shows that a net heat flux reversal occurred in the 21-second time in-

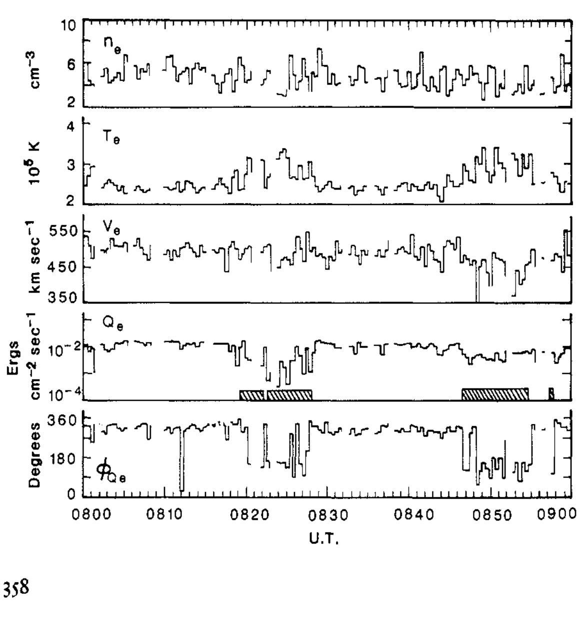

Fig. 4. Inbound upstream values of electron density, temperature, speed, heat flux, and heat flux direction.

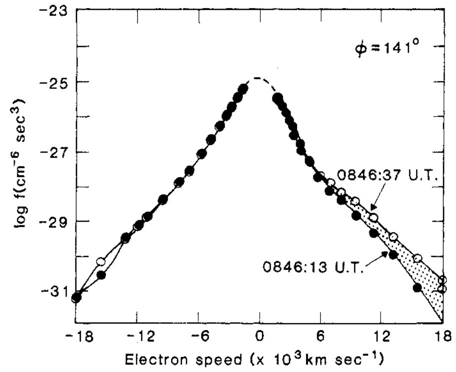

Fig. 5. Cuts taken along the heat flux direction (equivalent to the magnetic field direction) through two velocity distributions measured 24 seconds apart at the times shown. Negative speeds are outward from the sun. The elevated tail at positive speeds in the cut at 0846:37 U.T. is caused by magnetic connection to the hot transition region and produces a reversal in the net heat flux direction.

terval between two measurement cycles. The temperature is higher during the connection events, as is expected from addition of hot electrons from the comet transition region to the relatively cool solar wind electron population. Significant slowing of the solar wind occurred during the second event (Fig. 4).

Upstream density fluctuations. As ICE approached the comet and receded, almost continuous density fluctuations with periods of 2 to 4 minutes were observed in the solar wind. Numerous examples with peak-to-valley ratios of ~2 are evident in Fig. 4. Careful inspection of individual distributions demonstrates the validity of the variations. Fluctuations were detected at least 2×10^5 km upstream on either side of the comet, both during direct magnetic connection to the transition region, as inferred by return heat flux, and when there was no connection. If the density structures are convecting with the solar wind, then they have a size of ~60,000 km—comparable to but larger than the expected gyroradius of cometary ions, such as H_2O^+ and CO^+, picked up by the solar wind. We suggest that these upstream density fluctuations far from the comet are produced by an electromagnetic instability associated with solar wind pickup of cometary ions (*5*).

Table 1. Boundary crossing times and times and distances from closest approach at 1102:3 U.T. The transit speed was 20.9 km sec^{-1}. Regions are identified as SW (solar wind), TR (transition region), S (sheath), BL (boundary layer), IC (intermediate coma), and PT (developing plasma tail).

Boundary crossing	Crossing time (U.T.)	Time from closest approach (minutes)	Distance from closest approach ($\times 10^3$ km)
SW-TR	0920	−102	128
TR-S	1007	−55	69
S-BL	1050	−12.3	15
BL-IC	1056	−6.3	8
IC-PT	1101:1	−1.2	1.5
Center	1102:3	0	0
PT-IC	1103:5	1.2	1.5
IC-BL	1110	7.7	10
BL-S	1115	12.7	16
S-TR	1148	46	58
TR-SW	1220	78	98

Transition region and sheath. The transition region is an extended cometary region in which the incident solar wind and cometary plasma strongly interact to compress, heat, and slow the solar wind—apparently without the need for a small-scale bow shock. As described previously, n_{av} and T_{av} increased slowly toward the center in this region, while V_{av} decreased. Extending in from the inner boundary of the transition region was the sheath, in which n_{av} and T_{av} decreased toward the center while V_{av} continued its downward trend. In the transition region, V_{av} decreased nearly linearly to roughly half its upstream value, as predicted by theory (*12*). T_{av} increased by a factor of ~1.5 to 2 and n_{av} by a factor of ~2 to 3. In the sheath V_{av} continued to fall, reaching values below 10 percent of its upstream value, T_{av} decreased to near its upstream value, and n_{av} fell slightly from its peak value at the inner edge of the transition region.

The transition region and sheath were characterized by distinctly different spectral shapes. Examples of electron distributions measured in the two regions are given in Fig. 3. The transition-region distributions were characterized primarily by high variability, with some distributions upstream-like and others sheathlike. The upstream-like distributions were more frequent near the upstream edge, while the sheathlike distributions were more frequent near the inner edge, but there was no monotonic evolution from one to the other (Fig. 3). The sheath distributions had a characteristic "broken" spectral shape, being flatter at lower energies (Fig. 3). They were most often isotropic, as at 1122:07 U.T., but occasionally were anisotropic, as at 1137:43 U.T.

Both the transition region and the sheath were characterized by rapid and sometimes very large amplitude fluctuations in the plasma moments (Fig. 1). Several large density spikes, with widths of 1 to 2 minutes and peak-to-valley ratios in the range 2 to 7, are present in the data. Figure 6 shows 1 hour of data on an expanded time scale between 0920 and 1020 U.T. Although there is no completely consistent one-to-one correspondence between variations in T and n, frequently T is low when n is high or vice versa (for example, at ~0927 to ~0930 U.T., and at ~0931, ~0942, and ~1009 U.T.). In addition, examples can be found in Fig. 6 in which either the density or the temperature decreases at the same time that the other rises. This is of particular interest because such a change is distinctly different from that of a typical fast-mode shock transition, which is characterized by in-phase changes in both n and T. The possibility that these density and temperature fluctuations are due to a series of shocks seems to be ruled out. Indeed, on neither the inbound nor the outbound traversals was there any sharp transition with the clear fluid signature of a standing bow shock. Finally, while these high-density spikes in the transition

Table 2. Distances between outer boundaries and average thicknesses of the comet plasma regions along the encounter trajectory.

Region	Crossing distance ($\times 10^3$ km)	Thickness ($\times 10^3$ km)
TR	226	50
S	127	48
BL	31	6
IC	18	8
PT	3	3

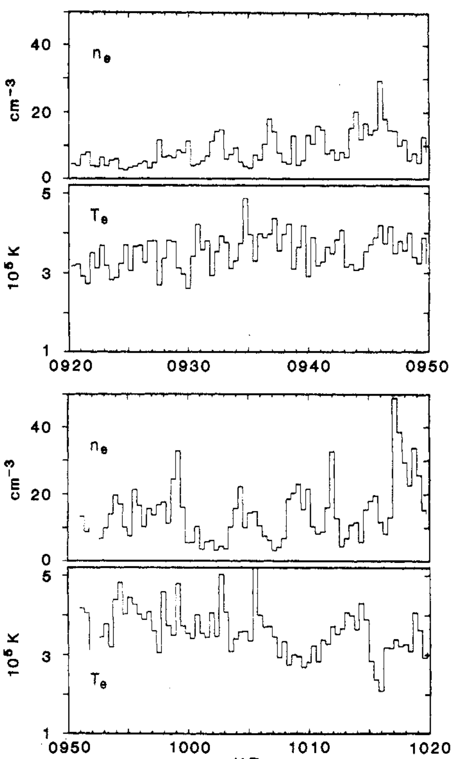

Fig. 6. Density and temperature values in the transition region and sheath during a period of 1 hour. Temperature and density are frequently anticorrelated in the transition region.

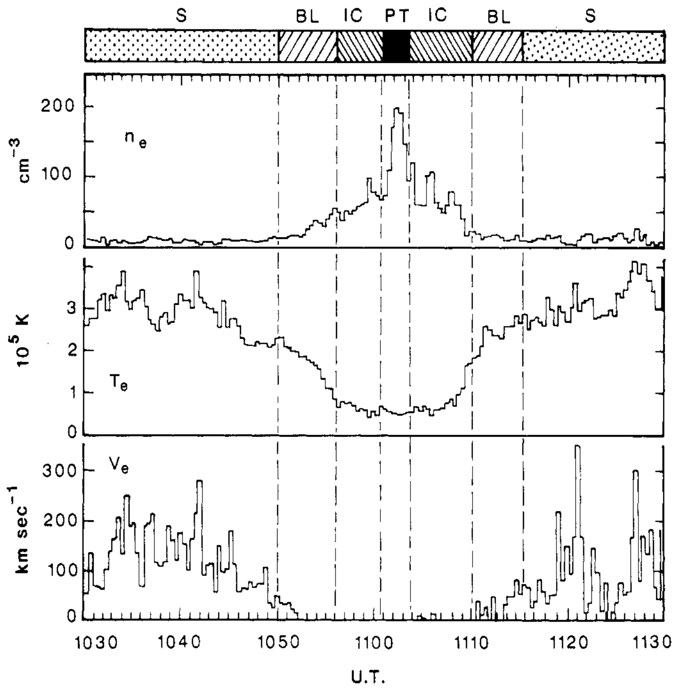

Fig. 7. Density, temperature, and flow speed during the hour centered on the time of closest approach.

region and sheath may be due to an instability associated with cometary ion pickup, as we suggest is the case for upstream density fluctuations, an alternative possibility is that they result from the passage of the spacecraft through cometary rays or streamers. If the structures are stationary in the comet frame, then they have a size of ~2000 km, comparable to the lateral dimensions of cometary rays observed in photographs (*13*).

Cold intermediate coma, boundary layer, and cold plasma tail. Inside the sheath was a cold intermediate coma. Figure 7 shows a moment plot for the period 1030 to 1130 U.T. that is centered on the time of closest approach to the nucleus. Close inspection shows that apparently there was a boundary layer separating the sheath from this intermediate coma. It seems that a diffuse contact surface, separating cometary and solar wind plasmas, may have been associated with this boundary layer.

In the boundary layer the temperature declined more rapidly than in the sheath and the plasma flow speed fell to zero. The accuracy of our standard analysis at low flow speeds is such that a value of 0 km sec^{-1} might be calculated when the true speed is <30 km sec^{-1}. The estimated extents of the boundary layer and other regions are shown by a coded bar at the top of Fig. 7. Inbound, the temperature fell from $\sim 2.1 \times 10^5$ K at ~1050 U.T. to $\sim 1.6 \times 10^5$ K at ~1056 U.T. Outbound it rose from $\sim 2.0 \times 10^5$ K at ~1110 U.T. to $\sim 2.6 \times 10^5$ K at ~1115 U.T. These temperature changes correspond to a gradual steepening of the low-energy portion of the spectrum until the break at mid-energies disappears (Fig. 3).

In the intermediate coma, density increased to even higher levels while the total integrated temperature fell to a shallow minimum of $\sim 4.4 \times 10^4$ K. This temperature had several components. Identification of an intermediate coma region is strengthened by comparing the observed electron densities with an expected r^{-n} dependence, where r is the distance from the comet nucleus and n should be between 1 and 2 (*14*). Figure 8 shows such a comparison with an r^{-2} fit. A least-squares fit to the inbound data alone, with the obvious density spikes excluded, gives $r^{-1.6}$, suggesting that this region is an inner part of the coma surrounding an inner coma close to the nucleus. However, until more detailed analyses of combined data sets are made, the possibility that this entire region is a developing plasma tail, with an embedded dense plasma component similar to the current sheet at Venus or the plasma sheet at Earth, should be kept open.

At the center of the intermediate coma was a region of extremely high electron density that extended ~1500 km on either side of closest approach. Our standard calculated densities, based on a three-Maxwellian fit to the observed distributions, extend above 200 cm^{-3}. We believe that the actual densities in this inner coma region are substantially higher, since higher densities were observed by the radio wave experiment, which is well adapted to making measurements in very dense regions independent of temperature (*15*).

To understand the probable source of this difference, it is only necessary to examine the electron velocity distributions shown on the right in Fig. 3. These distributions are remarkably different from the flat-topped distributions in the sheath. In the normal operating mode, our measurements extend down to only 10 eV, but every 68 minutes two "photoelectron" cycles with energies down to 1.9 eV are taken. Fortuitously, this photoelectron mode occurred while ICE was within the intermediate coma, providing insight into the nature of the cold plasma distributions. Figure 9 shows a one-dimensional cut through one of the two distributions at 1059:21 U.T. The cut shows why our density and temperature determinations in the developing plasma tail may have reduced accuracy. The distributions are composed of three components: a low-energy core, an intermediate-energy component, and a higher energy halo. There is no hint of any photoelectrons in this distribution, implying that the spacecraft potential was very near to zero, as would be expected in such a dense, cold plasma. This result also implies that ICE intercepted very little dust, since such impacts would increase the spacecraft potential. Maxwellian fits to the three com-

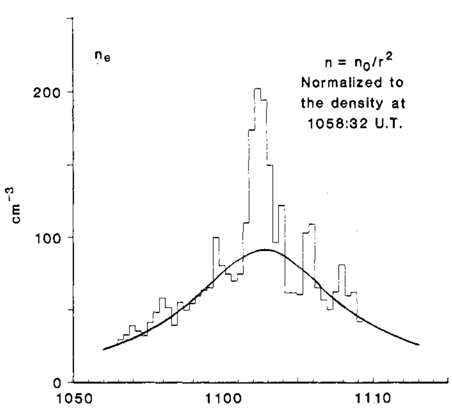

Fig. 8. Comparison of the intermediate coma electron density profile with an r^{-2} dependence.

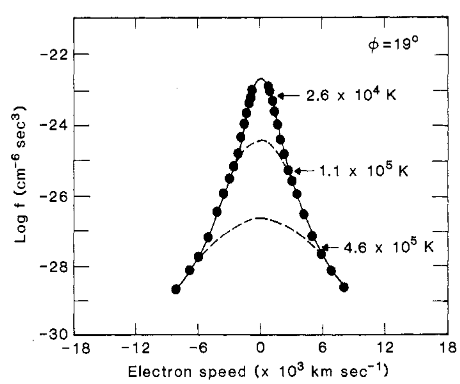

Fig. 9. Cut through a distribution measured in the photoelectron energy mode at 1059:21 U.T., showing a three-component distribution. Temperatures calculated by fitting the three components with Maxwellian distributions are shown.

ponents give temperatures of 2.6×10^4, 1.1×10^5, and 4.6×10^5 K. The total density for this distribution is ~ 100 cm^{-3}. All the measurements in the dense plasma tail (1101:20 to 1103:20 U.T.) were made in the normal mode, with energies extending down to only 10 eV. Obtaining accurate Maxwellian fits to the part of the distribution with lowest energy becomes a problem at these low temperatures without data points extending to lower energy values. In particular, if the plasma tail electron temperatures should fall to even lower values than in the adjacent inner coma where our photoelectron mode spectra were obtained, the calculated densities will be too low and total integrated temperatures too high. The intermediate distribution, shown in Fig. 9, found in the comet's cold intermediate coma may represent the electrons in the 20- to 30-eV energy range that are produced by photoionization of cometary molecules (*16*).

The plasma tail region in the center of the intermediate coma was exceptionally well defined (Fig. 7). With a single encounter it is not possible, of course, to determine the exact configuration of the dense plasma region, but since a two-lobed magnetic tail with neutral sheet was observed at the comet (*7*), this enhanced plasma may be the plasma or current sheet required in such a field-reversing magnetic topology. It may have a flattened slab or sheet configuration separating the two lobes, similar to the current sheet at Venus and the plasma tail in Earth's magnetotail. In the center of the plasma tail at Giacobini-Zinner we would expect to find an embedded neutral sheet. The enhanced density in the developing plasma tail should lead to decreased magnetic field strength through the diamagnetic effect.

In summary, the ICE encounter with comet Giacobini-Zinner revealed a strong solar wind–cometary plasma interaction. Many of the regions of the cometary tail postulated by theory were detected, but no evidence of a small-scale standing bow shock was found at the encounter distance behind the nucleus. Future explorations would be required to determine if a shock exists, for example, closer to the subsolar point of this comet. A recent study suggests that a bow shock might be absent on the flanks of a comet (*17*). We see evidence in the plasma electron data for electromagnetic instabilities associated with cometary ion pickup, possible cometary ray or streamer structures, the comet's cold intermediate coma surrounded by a boundary layer, and a developing cold plasma tail that is thought to be required by the draping magnetic topology. Other features of the comet, such as the existence of a contact surface, may emerge from future analyses of combined plasma and field data. We would expect the contact surface to be associated with the region that we have called a boundary layer.

REFERENCES AND NOTES

1. S. J. Bame *et al., IEEE Trans. Geosci. Electron.* **GE-16**, 160 (1978).
2. M. D. Montgomery, J. R. Asbridge, S. J. Bame, *J. Geophys. Res.* **73**, 4999 (1968).
3. K. W. Ogilvie, J. D. Scudder, M. Sugiura, *ibid.* **76**, 8165 (1971); W. C. Feldman, J. R. Asbridge, S. J. Bame, M. D. Montgomery, *ibid.* **78**, 3697 (1973).
4. S. J. Bame *et al., ibid.* **85**, 2981 (1980).
5. M. K. Wallis, *Nature (London)* **233**, 23 (1971).
6. N. F. Ness and B. D. Donn, *Mem. Soc. R. Liege Vol. Hors Ser. 5* **12**, 141 (1965).
7. E. J. Smith *et al., Science* **232**, 382 (1986).
8. H. Alfvén, *Tellus* **9**, 92 (1957).
9. C. T. Russell, J. G. Luhmann, R. C. Elphic, F. L. Scarf, *Geophys. Res. Lett.* **8**, 843 (1981); C. T. Russell, J. G. Luhmann, R. C. Elphic, M. Neugebauer, in *Comets*, L. L. Wilkening, Ed. (Univ. of Arizona Press, Tucson, 1982), p. 561; D. J. McComas, H. E. Spence, C. T. Russell, M. A. Saunders, *J. Geophys. Res.*, in press; J. A. Slavin, D. S. Intriligator, E. J. Smith, unpublished manuscript.
10. S. J. Bame, J. R. Asbridge, H. E. Felthauser, R. A. Olson, I. B. Strong, *Phys. Rev. Lett.* **16**, 138 (1966); S. J. Bame, J. R. Asbridge, H. E. Felthauser, E. W. Hones, I. B. Strong, *J. Geophys. Res.* **72**, 113 (1967); N. F. Ness, *ibid.* **70**, 2989 (1965).
11. W. F. Huebner, P. T. Giguere, W. L. Slattery, in *Comets*, L. L. Wilkening, Ed. (Univ. of Arizona Press, Tucson, 1982), p. 496.
12. H. U. Schmidt and R. Wegmann, *ibid.*, p. 538.
13. K. Wurm, *Astron. J.* **66**, 362 (1963).
14. W.-H. Ip and W. I. Axford, in *Comets*, L. L. Wilkening, Ed. (Univ. of Arizona Press, Tucson, 1982), p. 588.
15. N. Meyer-Vernet *et al., Science* **232**, 370 (1986).
16. J. S. Lee, J. P. Doering, T. A. Potemra, L. H. Brace, *Planet. Space Sci.* **28**, 973 (1980).
17. M. K. Wallis and M. Dryer, *Nature (London)* **318**, 646 (1985).

18. We thank P. Corrigan and R. Wales and other members of the ICE project staff for pleasant and professional support during this remarkable third phase of the International Sun-Earth Explorer 3 mission. Without the ingenious and remarkable peregrinations of ICE devised by R. Farquhar, this mission would never have happened. The science planning, headed by project scientist T. von Rosenvinge, made our participation in the mission a pleasure. We also appreciate the support of our Los Alamos co-workers, particularly S. Kedge and J. Goetzinger.

20 November 1985; accepted 31 January 1986

Observations of Energetic Ions from Comet Giacobini-Zinner

R. J. Hynds, S. W. H. Cowley, T. R. Sanderson, K.-P. Wenzel, J. J. Van Rooijen

During the encounter with comet Giacobini-Zinner, the energetic particle anisotropy spectrometer on the International Cometary Explorer spacecraft observed large fluxes of energetic ions, believed to result principally from ionization of the cometary atmosphere followed by pickup and acceleration by the ambient flow of the solar wind. These heavy cometary ions were observed from approximately 1 day before closest approach to about 2½ days afterward. Three regimes of differing ion characteristics have been identified. An outer region with a scale of $\sim 10^6$ kilometers contains variable fluxes of antisolar-streaming pickup ions in the undisturbed solar wind. In the middle region, of $\sim 10^5$ kilometers, fluxes have less large-scale variability and broader angular and energy distributions. This region is separated from the outer zone by a sharp transition. The inner region has a scale of $\sim 10^4$ kilometers and is characterized by reduced fluxes and complex angular distributions.

More than 20 years have passed since it was predicted that the interaction between a cometary atmosphere and the solar wind would result in the production of large fluxes of energetic heavy ions in a large volume surrounding the nucleus of the comet (*1, 2*). Neutral atoms and molecules sublimating from the cometary nucleus expand outward, unrestrained by any significant gravitational attraction, at speeds of ~ 1 km sec^{-1}. They are then photoionized by solar ultraviolet radiation or by charge exchange with solar wind ions on characteristic time scales of $\sim 10^6$ seconds, creating an ion distribution extending $\sim 10^6$ km around the comet. On ionization, the newly created ions start cycloidal motion in the crossed electric and magnetic fields of the solar wind, thereby gaining energy proportional to their mass. For typical solar wind velocities the maximum energy gain is a few kiloelectron volts per atomic mass unit. Thus, for an ion in the "water group" (O^+, OH^+, and H_2O^+), expected to be the predominant ions, peak energies of some tens of kiloelectron volts are to be expected.

Acceleration of these heavy ions extracts energy from the solar wind plasma, so that,

R. J. Hynds and S. W. H. Cowley, Blackett Laboratory, Imperial College, London SW7 2BZ, United Kingdom.
T. R. Sanderson and K.-P. Wenzel, Space Science Department of European Space Agency, European Space Research and Technology Centre, Noordwijk, Netherlands.
J. J. Van Rooijen, Space Research Laboratory, Sterrekundig Institute, Utrecht, Netherlands.